Supporting Information

Highly exposed surface pore-edge FeN$_x$ sites for enhanced oxygen reduction performance in Zn-air batteries

Xiangyu Lu[a], Lihui Xiao[a], Peixia Yang*[a], Hao Xu[a], Lilai Liu[b], Ruopeng Li[a], Yaqiang Li[a], Huiling Zhang[a], Jinqiu Zhang[a], Maozhong An[a].

[a]MIIT Key Laboratory of Critical Materials Technology for New Energy Conversion and Storage, School of Chemistry and Chemical Engineering, Harbin Institute of Technology, Harbin, 150001 China.
[b]College of Environmental and Chemical Engineering, Heilongjiang University of Science and Technology, Harbin, 150022, China.

* Corresponding authors: Peixia Yang (yangpeixia@hit.edu.cn)

Experimental Section

Electrochemical Measurements

The electrochemical test were conducted by using a CHI-760e electrochemical station. A rotating disk electrode (RDE) and a rotating ring-disk glass carbon electrode (RRDE) were used as the working electrode. A Hg/HgO (alkaline medium) or Hg/Hg$_2$SO$_4$ (acidic medium) electrode and a graphite sheet electrode were used as reference and counter electrodes, respectively.

In order to the RHE, a two-electrode (Pt coil and the reference electrode) were connected to be calibrated. Ultrapure hydrogen gas was sparged into the electrolyte for 10 minutes. As a result, H$^+$/H$_2$ equilibrium was established on the Pt coil, which thus acted as a RHE. A stable open circuit voltage could be tested for several minutes, which was taken to be the conversion value. The calibration values were E(RHE)= E(Hg/HgO)+0.896 V in 0.1 M KOH and E(RHE)= E(Hg/Hg$_2$SO$_4$)+0.716 V in 0.1M HClO$_4$, respectively.

ORR activity was measured by cyclic voltammetry (CV) at a scan rate of 50 mV·s^{-1} and linear sweep voltammetry (LSV) with 1600 rpm at a scan rate of 10 mV·s^{-1} in 0.1 M KOH saturated with O$_2$/N$_2$. The accelerated durability test (ADT) was investigated by continuous potential cycling from 0.6 to 1.0 V at a scan rate of 50 mV·s^{-1}.

The the rotating ring disk electrode (RRDE) was used to measure the hydrogen peroxide yield (H$_2$O$_2$%) and the number of electron transfers (n) according to the following equation:

$$H_2O_2(100\%) = 200\frac{I_R/N}{I_D + I_R/N}$$

$$n = 4\frac{I_D}{I_D + I_R/N}$$

where I_D is expressed as the disk current density, I_R is expressed as the ring current density, and N is expressed as the collection efficiency of the Pt ring (37%).

Density functional theory (DFT) calculations

DFT calculations were performed using Dmol3 of Materials studio. The layer of graphene 7×7 sheet as the model of graphene and the vacuum space above these sheets were taken to be 20 Å. The Perdew-Burke-Ernzerhof (PBE) functional with the basis set of the double numerical atomic orbital plus the polarization function (DNP) is adopted. The simulation of the water environment for Zn-air batteries cathode catalyst were performed with Cosmo and the dielectric constant is set to 78.54. The convergence tolerances of energy, maximum displacement, and maximum displacement were 1.0×10^{-5} Ha, 0.005 Å, 0.002 Ha Å^{-1}, respectively. The smearing value was set at 0.005 Ha to accelerate the energy convergence speed.

The adsorption energy (E_{ads}) of ORR intermediates is calculated as follows:

$$E_{ads} = E_{total} - E_o - E_{sub}$$

where the E_{total} is total adsorption energy of the catalyst and species, E_{sub} is the catalyst energy without adsorption, and E_o is the energy of the species.

The pathways on Fe$_4$N supported N-C systems were calculated in detail according to electrochemical framework developed by Nørskov. The free energy change of every elementary reaction is calculated as follows:

$$\Delta G = \Delta E + T\Delta S + \Delta ZPE + \Delta G_{field} + \Delta G_U + \Delta G_{pH}$$

Where ΔE is the reaction energy change, T is the temperature (289.15 K), ΔS is the vibrational entropy change, and ΔZPE is the zero point energy, respectively. The parameters of ΔZPE and ΔS can be calculated according to the vibration frequency of oxygen-contained intermediates.The influence of electric potential on the Gibbs free energy is expressed by ΔG_U=-neU, where n is the number of electrons transferred and U is the electrode potential. In this study, ΔG_{pH} and ΔG_{field} are not involved because they have less contribution to the trends of free energy change.

Preparation and tests of Zn-air batteries

The Liquid Zn-air battery was assembled with a uniform nickel foam coated with catalyst ink as an air cathode, 6 M KOH and 0.2 M CH$_3$COO)$_2$Zn as the electrolyte, and a polished Zn plate as an anode. 2.5 mg of catalyst, 1 mg of acetylene black, and 4 mg of activated carbon was added to the mixed solution containing 8 μL of Nafion and 200 μL of isopropanol. Subsequently, the uniform catalyst ink was applied dropwise to the surface of nickel foam as an air cathode. The polarization curves of the batteries were collected using the CHI760E electrochemical workstation in an air environment. The performance of batteries was tested by the LAND CT2001A test system. The discharge-charge cycling stability of the battery at 5 mA cm^{-2} with 10 min per cycle.
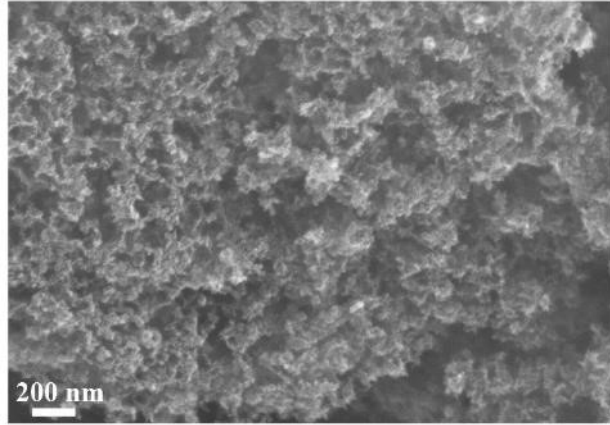
Fig. S1. SEM of FeN$_x$-HPNC.
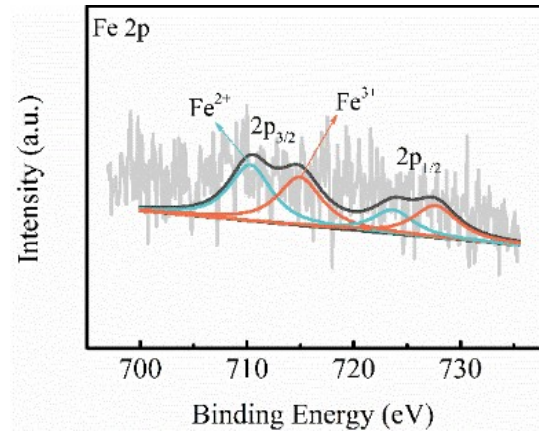
Fig. S2. Fe 2p XPS spectrum of SPE-FeN$_x$-HPNC
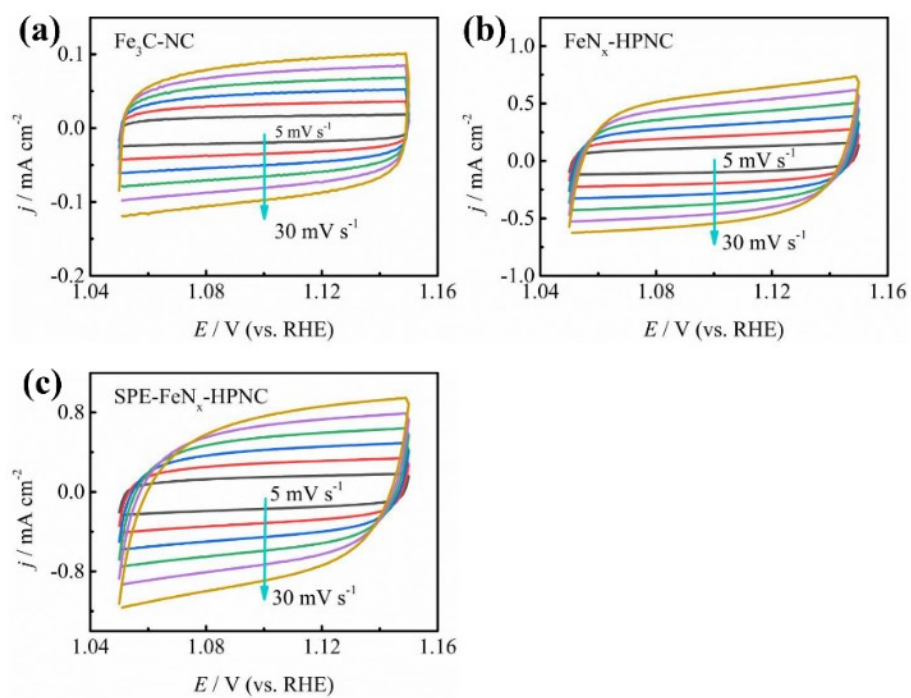
Fig. S3. CV curves of (a) Fe₃C-NC, (b) FeNₓ-HPNC and (c) SPE-FeNₓ-HPNC, respectively, at various scan rates (5, 10, 15, 20, 25, and 30 mV/s).
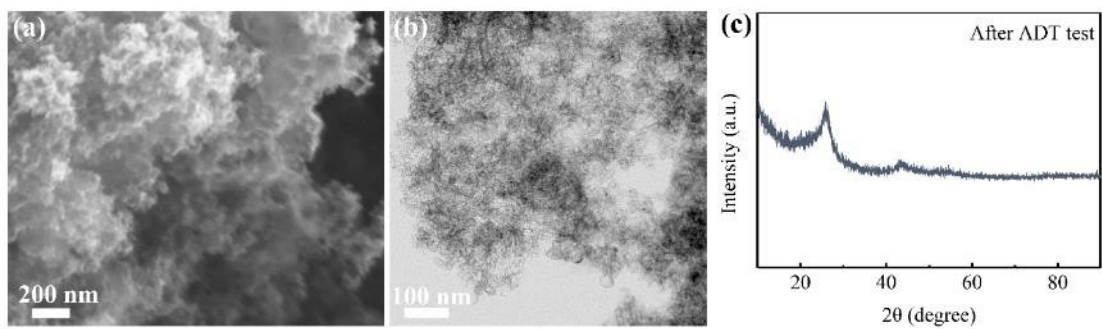
Fig. S4. (a) SEM image, (b)TEM image, (c) XRD pattern of SPE-FeN$_x$-HPNC after durability test.
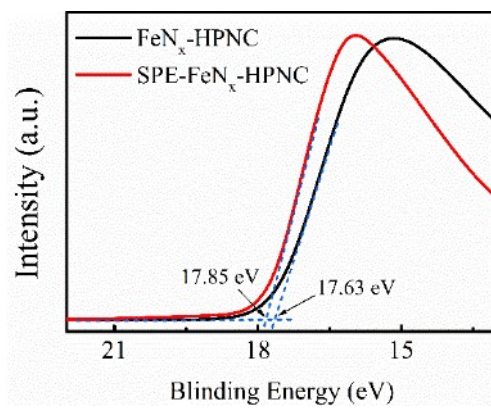
Fig. S5. Ultraviolet photoelectron spectroscopy analysis of FeN_x-HPNC and SPE-FeN_x-HPNC.
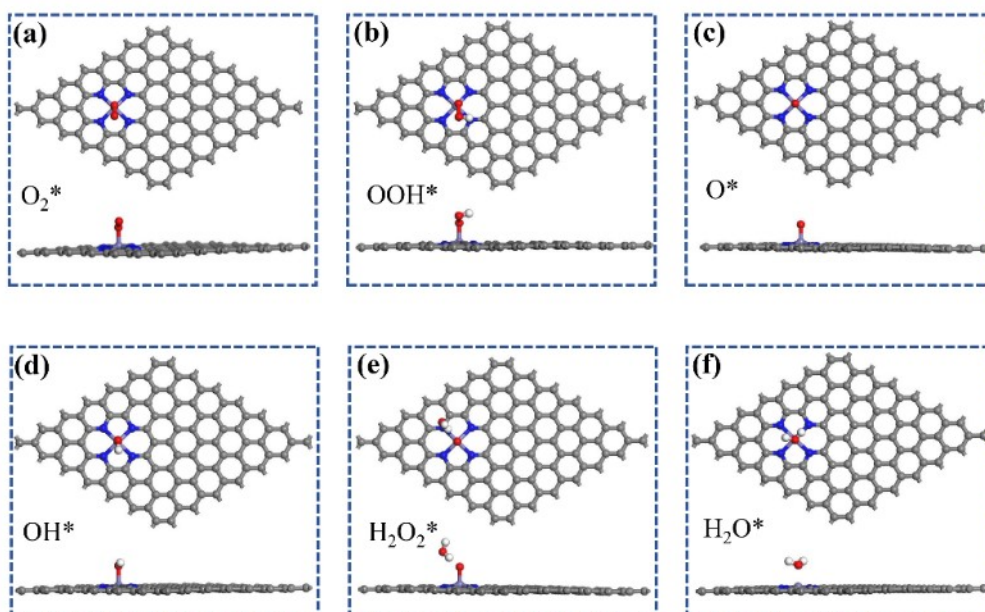
Fig. S6. Structure of the adsorption configurations of the ORR intermediates on the FeN$_x$ site where gray, blue, red, and white balls represent carbon, iron, oxygen, and hydrogen atoms.
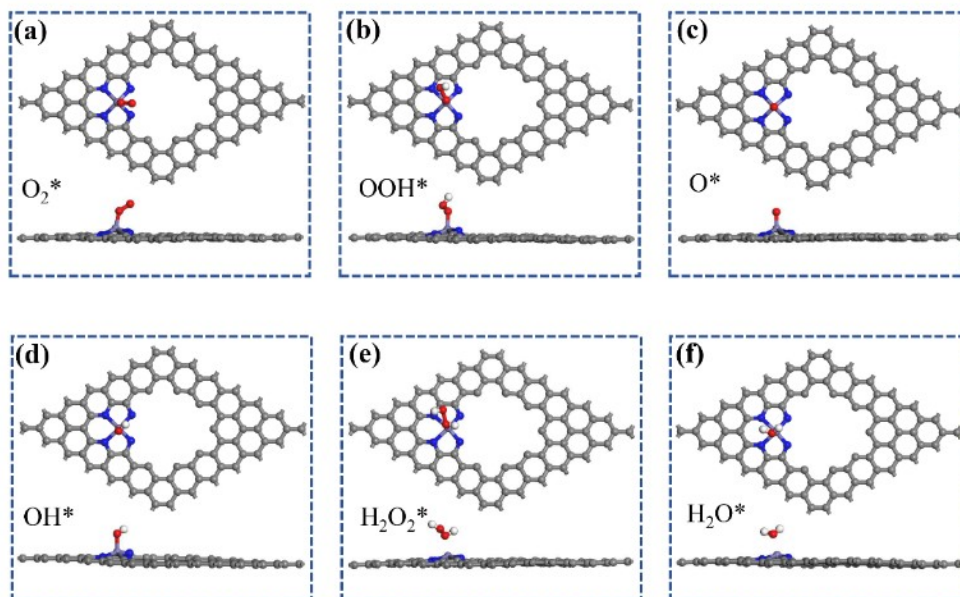
Fig. S7. Structure of the adsorption configurations of the ORR intermediates on the pore-edge FeN_x site where gray, blue, red, and white balls represent carbon, iron, oxygen, and hydrogen atoms.

Table S1. Specific surface area and pore parameters of as-prepared materials.

Catalysts	Specific surface area (m^2 g^{-1})	Pore volume (cm^3 g^{-1})	Average pore diameter (nm)
Fe$_3$C-NC	198.72	0.2785	5.4144
FeN$_x$-HPNC	831.65	2.4224	15.5145
SPE-FeN$_x$-HPNC	737.18	2.1722	15.1258

Table R2. Pore structure data from the N$_2$ adsorption/desorption isothermal measurements.

	Fe$_3$C-NC	FeN$_x$-HPNC	SPE-FeN$_x$-HPNC
S-total (cm^2 g^{-1})	199	832	737
S-micro (cm^2 g^{-1})	74.59	223	173
S-meso (cm^2 g^{-1})	124	609	564
S-micro%	37.5%	26.8%	23.4%
S-meso%	62.5%	73.2%	76.6%
V-total (cm^3 g^{-1})	0.27849	2.42243	2.17221
V-micro (cm^3 g^{-1})	0.09945	0.09417	0.07346
V-meso (cm^3 g^{-1})	0.17904	2.32826	2.09875
V-micro%	35.7%	3.9%	3.4%
V-meso%	64.3%	96.1%	96.6%

* The S represents the specific surface area and the V represents the pore volume.

Table S3. The content of C, N, O and Fe of the prepared catalysts obtained from XPS

Catalysts (at%)	C	N	O	Fe
Fe_3C-NC	94.3	1.27	4.32	0.11
FeN_x-HPNC	91	1.82	7.19	0.01
SPE-FeN_x-HPNC	91.91	1.91	6.07	0.11

Table S4. A comparison table of the ORR performance between this work and recently reported Pt-free catalysts in alkaline and acidic medium (vs. RHE)

Materials	$E_{1/2}$ (V) in 0.1 M KOH	$E_{1/2}$ (V) in 0.1 M $HClO_4$ or 0.5 M H_2SO_4	References
SPE-FeN_x-HPNC	0.902	0.754 ($HClO_4$)	This work
Cu-NSDC SACs	0.84	/	[1]
Fe_2-N/CNTs-850	0.846	/	[2]
Sb_1/NG(O)	0.86	/	[3]
ZnCu-N-C (1000)	0.87	/	[4]
NHC-900	0.835	/	[5]
Co@NrC-0.3	0.85	/	[6]
NSC/Co_9S_8-200	0.83	/	[7]
CuSA/CuCT@NPC	0.88	0.70 ($HClO_4$)	[8]
Fe/Ni(1:3)-NG	0.842	/	[9]
NC-Co SA	0.87		[10]
CoN4/NG	0.87	/	[11]
CoNi-SAs/NC	0.76	/	[12]
Fe/N-G#4	0.852	/	[13]
Fe–Nx ISAs/GHSs	0.89	/	[14]
NFC@Fe/Fe3C-9	0.87	0.73 ($HClO_4$)	[15]
NSPC-0.2–900	0.84	0.71 ($HClO_4$)	[16]

Table S5. A comparison table of the ORR durability between this work and recently reported Pt-free catalysts in alkaline medium.

13

Materials	$\triangle E_{1/2}$ in 0.1 M KOH	References
SPE-FeN$_x$-HPNC	8 mV (5000 cycles)	This work
Fe$_2$-N/CNTs-850	26 mV (3000 cycles)	[2]
Fe/Ni(1:3)-NG	23 mV (3000 cycles)	[9]
3D Fe/N-G#4	13 mV (3000 cycles)	[13]
Fe–Nx ISAs/GHSs	14 mV (5000 cycles)	[14]
NFC@Fe/Fe3C-9	16 mV (30000 cycles)	[15]
porous CS	10 mV (1000 cycles)	[17]

Table S6. Summary of the performance of aqueous and solid state ZABs based on Pt-free athode catalysts.

Materials	OCV of Aqueous ZABs (V)	Aqueous ZABs Peak power density (mW cm^2)	References
SPE-FeN$_x$-HPNC	**1.505**	**150**	**This work**
Fe$_{0.5}$Co@HOMNCP	1.619	134	[18]
Co/MnO@NC	1.5	146	[19]
NHC-900	1.345	107	[5]
NC-Co SA	1.41	/	[10]
CoN$_4$/NG	1.51	115	[11]
CoNi-SAs/NC	1.45	101.4	[12]
Fe-N-C-700	1.424	/	[20]

Reference

1.   H. Zhang, Q. Sun, Q. He, Y. Zhang, X. He, T. Gan and H. Ji, *Nano Research*, 2022, DOI: 10.1007/s12274-022-4289-3.
2.   C. Li, Y. Wu, M. Fu, X. Zhao, S. Zhai, Y. Yan, L. Zhang and X. Zhang, *ACS Applied Energy Materials*, 2022, **5**, 4340-4350.
3.   Y. Gu, B. Xi, H. Zhang, Y. Ma and S. Xiong, *Angew Chem Int Ed Engl*, 2022, DOI: 10.1002/anie.202202200.
4.   M. Qian, M. Guo, Y. Qu, M. Xu, D. Liu, C. Hou, T. T. Isimjan and X. Yang, *Journal of Alloys and Compounds*, 2022, **907**.
5.   L. Wang, S. Q. Guo, Z. Hu, B. Shen and W. Zhou, *ChemCatChem*, 2022, DOI: 10.1002/cctc.202200063.
6.   J. Yu, Y. Dai, Z. Zhang, T. Liu, S. Zhao, C. Cheng, P. Tan, Z. Shao and M. Ni, *Carbon Energy*, 2022, DOI: 10.1002/cey2.171.
7.   Q. Zheng, Y. Xiong, K. Tang, M. Wu, H. Hu, T. Zhou, Y. Wu, Z. Cao, J. Sun, X. Yu and C. Wu, *Nano Energy*, 2022, **92**.
8.   Z. Yang, K. Jiang, G. Tong, C. Ke, H. Wu, P. Liu, J. Zhang, H. Ji, J. Zhu, C. Lu and X. Zhuang, *Chemical Engineering Journal*, 2022, **437**.
9.   Y. Ma, H. Fan, C. Wu, M. Zhang, J. Yu, L. Song, K. Li and J. He, *Carbon*, 2021, **185**, 526-535.
10.   W. Zang, A. Sumboja, Y. Ma, H. Zhang, Y. Wu, S. Wu, H. Wu, Z. Liu, C. Guan, J. Wang and S. J. Pennycook, *ACS Catalysis*, 2018, **8**, 8961-8969.
11.   L. Yang, L. Shi, D. Wang, Y. Lv and D. Cao, *Nano Energy*, 2018, **50**, 691-698.
12.   X. Han, X. Ling, D. Yu, D. Xie, L. Li, S. Peng, C. Zhong, N. Zhao, Y. Deng and W. Hu, *Adv Mater*, 2019, **31**, e1905622.
13.   C. Wang, Z. Li, L. Wang, X. Niu and S. Wang, *ACS Sustainable Chemistry & Engineering*, 2019, **7**, 13873-13885.
14.   X. Qiu, X. Yan, H. Pang, J. Wang, D. Sun, S. Wei, L. Xu and Y. Tang, *Adv Sci (Weinh)*, 2019, **6**, 1801103.
15.   M. Karuppannan, J. E. Park, H. E. Bae, Y. H. Cho and O. J. Kwon, *Nanoscale*, 2020, **12**, 2542-2554.
16.   L. Wang, K. Liang, L. Deng and Y.-N. Liu, *Applied Catalysis B: Environmental*, 2019, **246**, 89-99.
17.   C. Su, Y. Liu, Z. Luo, J.-P. Veder, Y. Zhong, S. P. Jiang and Z. Shao, *Chemical Engineering Journal*, 2021, **406**.
18.   W. Li, B. Liu, D. Liu, P. Guo, J. Liu, R. Wang, Y. Guo, X. Tu, H. Pan, D. Sun, F. Fang and R. Wu, *Adv Mater*, 2022, **34**, e2109605.
19.   Y. Niu, X. Teng, S. Gong, X. Liu, M. Xu and Z. Chen, *Energy Storage Materials*, 2021, **43**, 42-52.
20.   T. Chen, J. Wu, C. Zhu, Z. Liu, W. Zhou, C. Zhu, C. Guan and G. Fang, *Chemical Engineering Journal*, 2021, **405**.